

Substrate-mediated umklapp scattering at the incommensurate interface of a monatomic alloy layerSantosh Chiniwar,¹ Angus Huang,¹ Ting-Yu Chen,¹ Chung-Huang Lin,¹ Cheng-Rong Hsing,² Wei-Chuan Chen,¹ Cheng-Maw Cheng,³ H.-T. Jeng,^{1,4,*} C. M. Wei,² Woei Wu Pai,^{5,6,†} and S.-J. Tang^{1,3,4,‡}¹*Department of Physics, National Tsing Hua University, Hsinchu 30013, Taiwan*²*Institute of Atomic and Molecular Sciences, Academia Sinica, Taipei 106, Taiwan*³*National Synchrotron Radiation Research Center (NSRRC), Hsinchu 30076, Taiwan*⁴*Institute of Physics, Academia Sinica, Taipei 11529, Taiwan*⁵*Center for Condensed Matter Sciences, National Taiwan University, Taipei 106, Taiwan*⁶*Department of Physics, National Taiwan University, Taipei 106, Taiwan*

(Received 26 October 2018; revised manuscript received 18 February 2019; published 8 April 2019)

Ultrathin Pb and Ge films deposited on Ag(111) surfaces have been investigated and compared. We found that at 1/3 ML, both films formed surface alloys, Ag₂Pb and Ag₂Ge, with $\sqrt{3} \times \sqrt{3}R30^\circ$ and $\frac{19}{20}\sqrt{3} \times \frac{19}{20}\sqrt{3}R30^\circ$ structures on Ag(111) but the surface electronic structures exhibit a most evident difference at the Ag(111) surface zone boundary $\bar{M}_{\text{Ag}(111)}$, where the single band and the splitting ones were observed, respectively. Up to 1 ML, Ag₂Ge subsequently develops into germanene with a striped phase and then a quasifreestanding phase, as previously reported [Lin *et al.*, *Phys. Rev. Mater.* **2**, 024003 (2018)], while Ag₂Pb evolves to a dense Pb(111) phase that also reveals splitting bands at $\bar{M}_{\text{Ag}(111)}$. We discover that the larger (smaller) atomic size of a Pb (Ge) atom with respect to an Ag atom causes the commensurate (incommensurate) interfaces and further demonstrate that the splitting bands of Ag₂Ge surface alloy and 1-ML Pb film originated from the commonly incommensurate interface with Ag(111), which mediates umklapp scattering by inducing the mirror image of the pristine Ag₂Ge and Pb(111) bands relative to $\bar{M}_{\text{Ag}(111)}$.

DOI: [10.1103/PhysRevB.99.155408](https://doi.org/10.1103/PhysRevB.99.155408)**I. INTRODUCTION**

Two-dimensional (2D) materials have been a research focus in recent years. 2D-xenes such as silicene [1,2], germanene [3,4], stanene [5,6], borophene [7,8], bismuthine [9], and transition metal dichalcogenides monolayers (TMD), such as MoS₂ [10], WS₂ [11], MoSe₂ [12], WSe₂ [13,14], MoTe₂ [15], are considered as 2D topological insulators and 2D semiconductors with major potential for industrial applications. For TMD, the bonding is a mainly weak van der Waals type so the epitaxial layer grows with the lattice constants of their bulk structure in spite of large lattice mismatch at the interface. The condition for epitaxial growth of xenes on substrates is stricter than the commensurate interface suggested to be necessary [16], and the growth configurations are more varied. For example, germanene was found to have dual phases grown on Ag(111), that is, a striped phase (SP) and a quasifreestanding phase (QP) [3]. The former is uniaxially commensurate with the Ag(111)- $\sqrt{3} \times \sqrt{3}R30^\circ$ lattice (hereafter denoted as Ag- $\sqrt{3}$ -R30) and exhibits a well-ordered but tensile-strained honeycomb lattice; the latter is incommensurate with Ag(111) and reveals a twisted or imperfect honeycomb lattice. However, the intrinsic σ band of germanene was only observed in the latter [3]. Therefore, commensurability is not a necessary condition for growing a monatomic layer on a substrate, and incommensurability can even preserve

better the intrinsic electronic structures, such as σ bands, of a monolayer [3] due to a less effective interaction with the substrate. However, the π bands appear more vulnerable to the interaction with the substrate regardless of the commensurate or incommensurate interface [3,17,18]. The stability of a film was mainly investigated in terms of surface energies with a model of a freestanding slab, while the interfacial effect from the substrate was considered as a secondary factor [19]. However, when the film thickness reduces to one monolayer, the interfacial effect should become more relevant. Tang *et al.* [20] found that Pb films grown on Ge(111) are dominated by the configuration with 13% lattice mismatch at a thickness less than 2 ML. This was attributed to the stronger electron hybridization at the interface between the Pb film and Ge(111) substrate.

In this paper, we focus on surface alloys of Ag₂Ge [21,22] and Ag₂Pb [21,23] first, which are actually single alloy layers forming on the bulk Ag(111) surface. From the distinct features of electronic structures between the two surface alloys, mainly the splitting and nonsplitting surface state bands centered at $\bar{M}_{\text{Ag}(111)}$, we correlate this presence or absence of the band splitting to the corresponding incommensurate and commensurate interfaces of these two systems. Upon further deposition of Pb on Ag₂Pb/Ag(111), a dealloying process occurs; the commensurate Ag₂Pb/Ag(111) evolves into an incommensurate 1-ML dense Pb(111) layer on Ag(111) with its Pb band splitting at $\bar{M}_{\text{Ag}(111)}$, as well. The substrate-mediated umklapp scattering of the monolayer electrons at the interface is proposed to explain the observed band split and help the layer stability despite incommensurability.

*jeng@phys.nthu.edu.tw

†wpai@ntu.edu.tw

‡sjtang@phys.nthu.edu.tw

II. CALCULATIONAL METHODS AND EXPERIMENTAL PROCEDURES

The *ab initio* calculations are performed based on density functional theory (DFT) with the Vienna *Ab initio* Simulation Package (VASP) [24–26]. The Perdew-Burke-Ernzerhof [27] generalized-gradient-approximation functional and projector augmented wave [28,29] method are adopted in the self-consistent calculations. Two calculation approaches were employed in this paper: (1) The model of surface alloys on Ag slabs: The Ag_2Ge or Ag_2Pb alloy was formed on the double side surfaces with a repeating slab of 20 Ag layers and a vacuum region of ~ 26 Å. The theoretical optimized lattice constant of 4.146 Å for the Ag slabs was used, and Ge, Pb, and Ag atoms were allowed to fully relax except that the four Ag layers in the middle were fixed at their bulk positions. The plane-wave kinetic cutoff energy was 300 eV and the force on each atom was less than $0.005 \text{ eV \AA}^{-1}$. (2) The model of freestanding layers: The energy cutoff of 400 eV (400 eV) and k mesh of $12 \times 12 \times 1$ ($24 \times 24 \times 18$) were used in free-standing Ag_2Ge and Pb-1ML (Ag bulk). The DFT + Hubbard U , local-density approximation + U , method [30] with $U = 4.0 \text{ eV}$ and $J = 0.4 \text{ eV}$ [3] are applied on the Ag- d orbital to correct the binding energy of the Ag- d bands in Ag_2Ge and Ag bulk. To simulate the influence of umklapp scattering to the electronic bands, the band structures of Ag_2Ge and Pb 1-ML were unfolded back to the high-symmetry lines in the Ag(111) first Brillouin zone (See Supplemental Material Fig. S1 [31]). We also simulate the low energy electron diffraction (LEED) result of the Ag(111) surface with 2D hexagonal lattice parameter 2.88 Å (equal to 4.073 Å for the face-centered-cubic lattice). For the Ag_2Ge alloy, we use the lattice parameter of 4.7489 Å with a rotation angle of 30° (R30°). In comparison with $\text{Ag}\sqrt{3}\text{-R30}$, the lattice mismatch is -5% . On the other hand, for the 1-ML Pb, the lattice parameter 3.4 Å is used.

The experiment was performed in an ultrahigh vacuum system, where angle-resolved photoelectron spectroscopy (ARPES) and LEED were used. The single-crystal Ag(111) surface was cleaned by repeated cycles of sputtering with Ar^+ ions at 1.5 keV followed by annealing at 500° C until its cleanliness was verified by a sharp LEED diffraction pattern as well as the presence of a sharp L-gap Shockley surface state in the ARPES spectra. Ultrathin films of Pb and Ge were grown on Ag(111) substrates at room temperature (RT) and 100° C , respectively using an K-cell evaporator. ARPES data was collected from beamline 21B1-U9 at the National Synchrotron Radiation Research Center in Taiwan with a Scienta R4000 energy analyzer using p -polarized light at 27 eV, and with Scienta R3000 energy analyzer using mainly unpolarized He-I α light source at 21.2 eV. The energy and angular resolutions for the former (the latter) were 10 meV and 0.3° (30 meV and 0.4°).

III. RESULTS AND DISCUSSION

Figures 1(a) and 1(b) show the measured energy band dispersions of Ag_2Pb and Ag_2Ge surface alloys formed on the Ag(111) surface in the symmetry direction $\bar{\Gamma} - \bar{K} - \bar{M}$ ($\bar{\Gamma}_{\text{Ag}(111)} - \bar{M}_{\text{Ag}(111)}$) in terms of $\text{Ag}\sqrt{3}\text{-R30}$ and Ag(111)

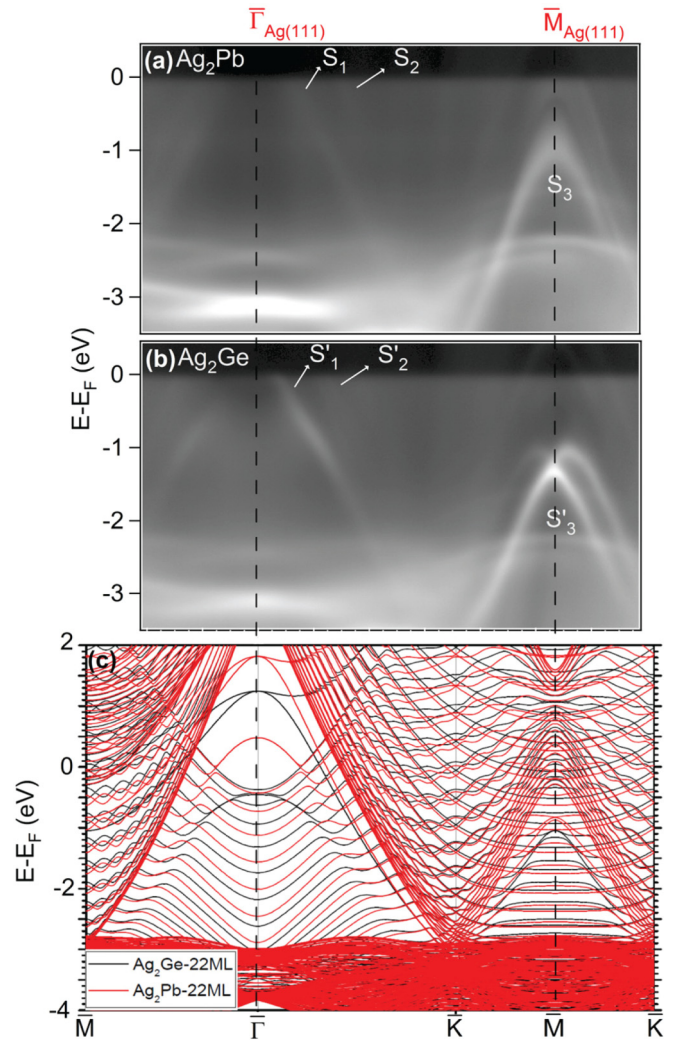


FIG. 1. Comparison between experimentally measured and calculated electronic structures of surface alloy layers formed on Ag(111) surface. (a), (b) Measured energy band structures of Ag_2Pb and Ag_2Ge using unpolarized light with 21.2 eV photon energy. $\bar{\Gamma}_{\text{Ag}(111)}\bar{M}_{\text{Ag}(111)} = 1.25 \text{ \AA}^{-1}$. (c) DFT calculation of band structures for Ag_2Ge and Ag_2Pb layer on a 22-layer Ag Slab.

surface Brillouin zones (SBZs), respectively. At the surface zone center $\bar{\Gamma}$, as reported by previous studies [21–23], unoccupied surface states (S_1 , S_2 , S'_1 , S'_2) were identified to disperse downward crossing Fermi levels for both surface alloys; those of Ag_2Pb surface alloys were especially shown to exhibit Rashba splitting with Rashba constant $1.42 \text{ \AA} \text{ eV}$ [23]. At the surface zone boundary (SZB) \bar{M} , the difference between the Ag_2Pb and Ag_2Ge surface alloys is more evident that the surface state band, S'_3 , at about -1.24 eV of the latter is splitting rather than the single one, S_3 , at about -0.95 eV in the former within the bulk projected Ag band gap. The split of the Ag_2Ge surface state band at \bar{M} was speculated to be caused by Rashba effects or structure disorder [21,22]. The nearly flat bands ranging about -3 eV in both Figs. 1(a) and 1(b) and the weak replica at about -2 eV are from Ag d electrons emitted by He-I β and γ , $h\nu = 23.09$ and 23.74 eV . Figure 1(c) shows the DFT calculation results for both surface

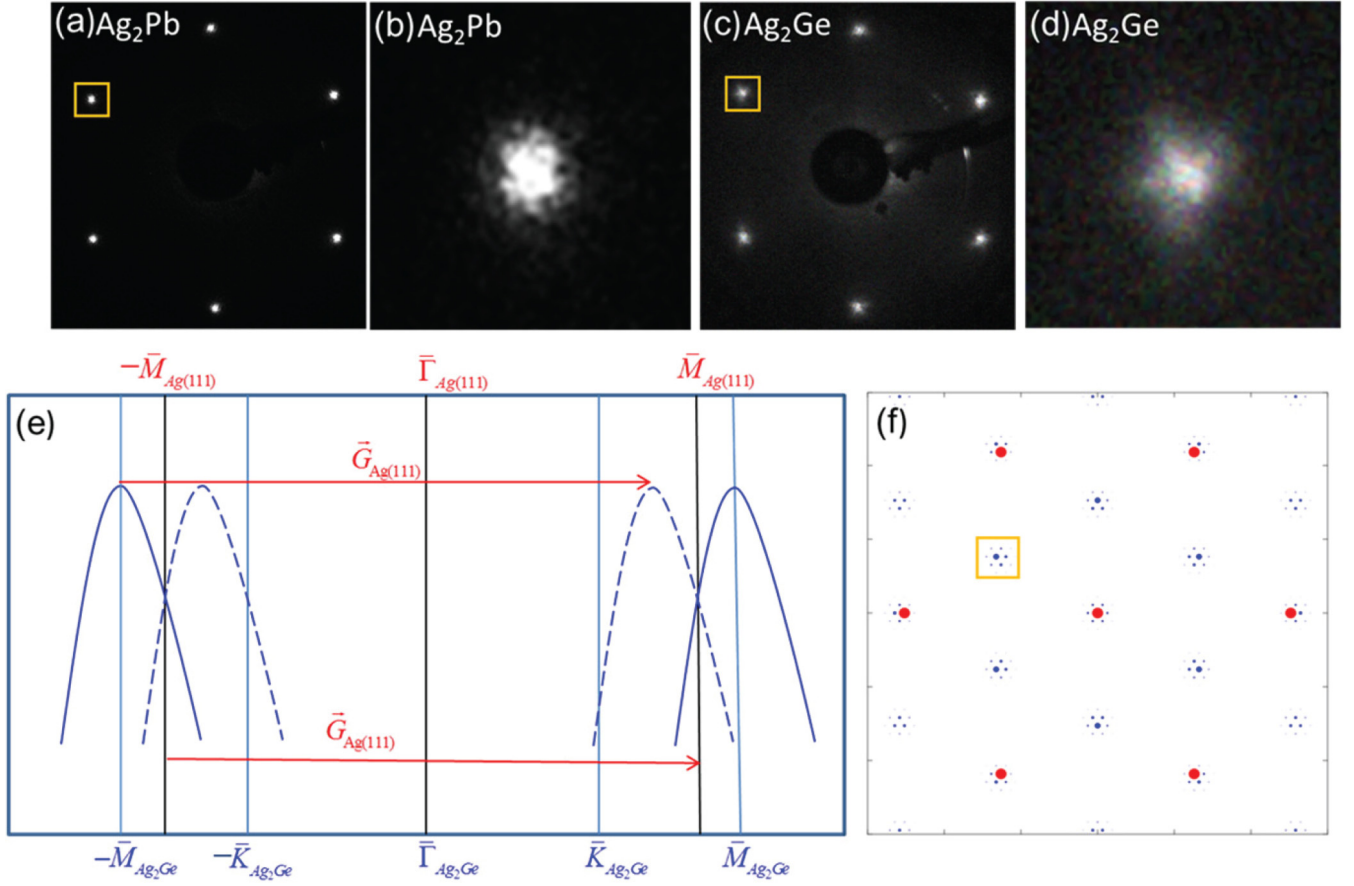


FIG. 2. Comparison of LEED patterns between Pb_2Ge and Ag_2Pb surface alloy on $\text{Ag}(111)$ using 20 eV electron energy. (a) LEED patterns of Pb_2Ge on $\text{Ag}(111)$ (b) The magnified view of the LEED spot enclosed in (a). (c) LEED patterns of Ag_2Ge on $\text{Ag}(111)$. (d) The magnified view of the LEED spot enclosed in (c). (e) Schematic to illustrate the umklapp scattering model for energy band splitting at $\bar{M}_{\text{Ag}(111)}$. (f) Simulated LEED patterns corresponding to (c). Blue and red denote Moiré and $\text{Ag}(111)$ spots.

alloys based on the model of the alloy layers on Ag slabs of 22 ML. The lattices of both alloy layers are considered to be commensurate with $\text{Ag}\sqrt{3}\text{-R}30$ in the calculation. Via a close comparison, the calculated surface state bands match the measured ones at $\bar{\Gamma}$ and \bar{M} reasonably well for PbAg_2 but disagree with the measured ones for Ag_2Ge in that the calculated S'_1 surface state at $\bar{\Gamma}$ is yet below the Fermi level, and moreover, the calculation cannot reproduce the S'_3 band split at \bar{M} . It is obvious that the calculation model employed fits Ag_2Pb rather than Ag_2Ge . What is the essential difference between them and what factor was not considered in the calculation?

Figures 2(a) and 2(c) show the LEED patterns of Ag_2Pb and Ag_2Ge on $\text{Ag}(111)$, taken at the same electron energy 20 eV. The six $(1/3\ 1/3)$ spots in both patterns correspond to the $\text{Ag}\sqrt{3}\text{-R}30$ lattice. Although the spot positions of the two surface alloys are identical, the spot shapes appear different; the former [Fig. 2(b)] look like filled circles, while the latter [Fig. 2(d)] exhibit satellite-like configuration around $(1/3\ 1/3)$ spots like Moirés. This implies that there is lattice mismatch between the Ag_2Ge layer and $\text{Ag}(111)$, which was overlooked in the calculation for Fig. 1(c). A typical Ag_2M surface alloy normally assumes the underlying $\text{Ag}\sqrt{3}\text{-R}30$ lattice, especially when the foreign atom M is of a similar size to the Ag atom. The radius of Pb, Ge, and, Ag atoms

are 1.8, 1.25, and 1.6 Å, respectively [32], so upon the Ag_2Pb alloy formation, a Pb atom, due to its larger size, can only be partially immersed into the top Ag layer until the alloy lattice is commensurate with $\text{Ag}\sqrt{3}\text{-R}30$. This is consistent with a previous LEED IV study showing that the top layer is corrugated such that the Pb atoms reside about 0.4 Å above the Ag atoms [33]. However, for a Ge atom, due to its much smaller size, the lattice of Ag_2Ge further contracts to a smaller value than that of $\text{Ag}\sqrt{3}\text{-R}30$. Therefore in Fig. 1(b), the right branch, with higher intensity, of the splitting bands centered at $\bar{M}_{\text{Ag}(111)}$ can be the original surface-state band of Ag_2Ge and the left branch, with lower intensity, is generated simply due to umklapp scattering via a $\text{Ag}(111)$ reciprocal lattice. This is consistent with the formation of Moiré LEED spots as linear combinations of the reciprocal vectors of the film and the substrate [3] namely,

$$\vec{k} = n_1 \vec{G}_{\text{Ag}_2\text{Ge}} + n_2 \vec{G}_{\text{Ag}(111)} (n_1 \text{ and } n_2 \text{ are integers}). \quad (1)$$

Figure 2(e) illustrates the model for explaining the energy band split at $\bar{M}_{\text{Ag}(111)}$ using substrate-mediated umklapp scattering, where $\bar{M}_{\text{Ag}_2\text{Ge}}$ is the SZB of the Ag_2Ge surface alloy with the contracted lattice from the $\text{Ag}\sqrt{3}\text{-R}30$ unit cell. The solid bands centered at the momentum of $-\bar{M}_{\text{Ag}_2\text{Ge}}$ and $\bar{M}_{\text{Ag}_2\text{Ge}}$ are identical due to the inversion symmetry of the

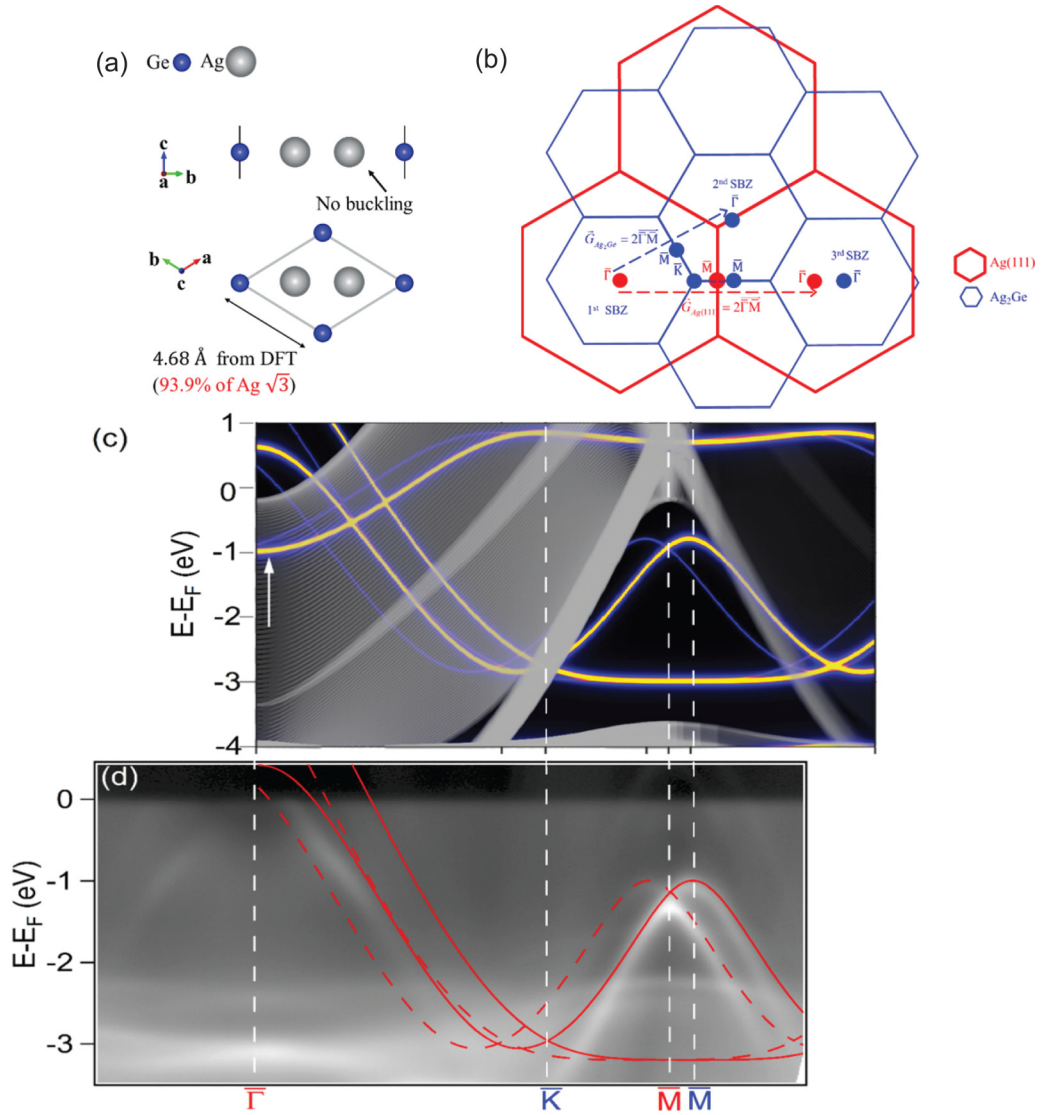


FIG. 3. Comparison between measured and calculated electronic structures for Ag₂Ge surface alloy. (a) Schematics (side and top view) to illustrate the model for DFT calculation of a freestanding layer of Ag₂Ge. (b) SBZs and symmetry points of the Ag₂Ge layer (denoted in blue) and the Ag(111) surface (denoted in red). $\bar{\Gamma}\bar{M}_{\text{Ag}(111)} = 1.25 \text{ \AA}^{-1}$, $\bar{\Gamma}\bar{K}_{\text{Ag}_2\text{Ge}}\bar{M}_{\text{Ag}_2\text{Ge}} = 1.31 \text{ \AA}^{-1}$, $\bar{\Gamma}\bar{K}_{\text{Ag}_2\text{Ge}} = 0.87 \text{ \AA}^{-1}$. (c) The calculated energy bands of freestanding Ag₂Ge derived from the model in (a). (d) Superimposition of DFT calculated band structures in (c) onto experimentally measured energy band dispersions in Fig. 1(b).

band structures. The dashed band translated from the one at $-\bar{M}_{\text{Ag}_2\text{Ge}}$ by umklapp scattering must be symmetrized with the band at $\bar{M}_{\text{Ag}_2\text{Ge}}$ with respect to $\bar{M}_{\text{Ag}(111)}$ simply because $\vec{G}_{\text{Ag}(111)} = 2\bar{\Gamma}_{\text{Ag}(111)}\bar{M}_{\text{Ag}(111)}$. The value of lattice mismatch (LM) can be extracted by the magnitude of the splitting, $|\bar{M}_{\text{Ag}(111)}\bar{M}_{\text{Ag}_2\text{Ge}}|$, namely,

$$\text{LM} = \frac{a_{\text{Ag}_2\text{Ge}} - a_{\text{Ag}(111)} - \sqrt{3} \times \sqrt{3}R30^\circ}{a_{\text{Ag}(111)} - \sqrt{3} \times \sqrt{3}R30^\circ} = \frac{\bar{M}_{\text{Ag}(111)}\bar{M}_{\text{Ag}_2\text{Ge}}}{\bar{\Gamma}_{\text{Ag}(111)}\bar{M}_{\text{Ag}_2\text{Ge}}} \quad (2)$$

and the deduced value is -5% from the measured band split, 0.064 \AA^{-1} , in Fig. 1(b). The corresponding Wood notations for the Ag₂Ge layer and Moiré pattern are $\frac{19}{20}\sqrt{3} \times \frac{19}{20}\sqrt{3}R30^\circ$ and $19\sqrt{3} \times 19\sqrt{3}R30^\circ$, respectively. With the corresponding

lattice constants to the extracted value, the Moiré spots are reproduced using Eq. (1), as shown in Fig. 2(f). The yellow square encloses the Moiré spots around (1/3 1/3). The measured counterparts [Fig. 2(d)] are not clearly resolved. As previously reported [3], above 1/3 ML, the dealloying process starts engaging to form a complete SP at about 0.74 ML. It is possible that some precursors of SP already coexist with the Ag₂Ge alloy at 1/3 ML and effect the long-range order.

To further confirm this model, we employed a DFT calculation only considering a freestanding layer of Ag₂Ge as shown in Fig. 3(a). The fully relaxed lattice constant is 4.68 Å, 93.8% of that of an Ag√3-R30 unit cell. The corresponding lattice mismatch, -6.2% , is close to that extracted from the measured band splitting. The smaller LM magnitude in the real case, Ag₂Ge on Ag(111), is understandable in light of the fact that the underlying Ag substrate is resistant to the contraction

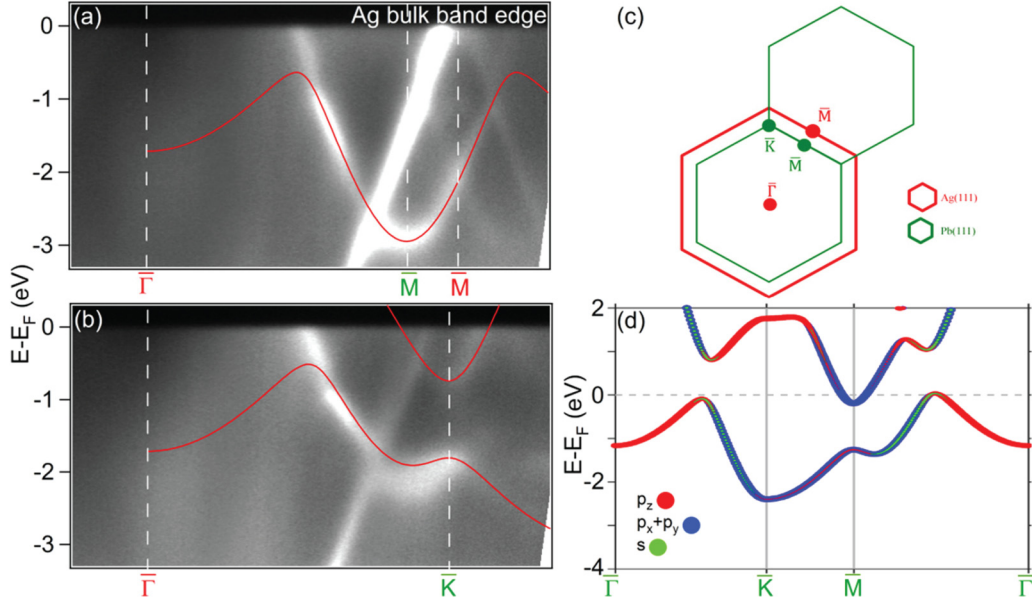


FIG. 4. Energy band structures for 1-ML Pb(111) dense phase on Ag(111). (a), (b) The measured energy band dispersion, taken at 27-eV photon energy, of 1-ML Pb(111)- 1×1 dense phase on Ag(111) in two symmetry directions with DFT calculated bands (red curves) superimposed from (d). (c) SBZs and symmetry points of Ag(111) (denoted in red) and 1-ML Pb(111) layer (denoted in green). $\bar{\Gamma}\bar{M}_{\text{Ag}(111)} = 1.25 \text{ \AA}^{-1}$, $\bar{\Gamma}\bar{M}_{\text{Pb}(111)} = 1.03 \text{ \AA}^{-1}$, $\bar{\Gamma}\bar{K}_{\text{Pb}(111)} = 1.19 \text{ \AA}^{-1}$ (d) DFT calculated energy bands of one-layer freestanding Pb in symmetry directions.

of Ag_2Ge from the $\text{Ag}\sqrt{3}\text{-R30}$ lattice. We, therefore, intentionally employed the lattice constant corresponding to -5% lattice mismatch for the band calculation of the freestanding Ag_2Ge layer, and then unfolded the calculated energy bands with the $\text{Ag}(111)$ reciprocal vector [See Supplemental Material Fig. S1 [31]]. The resulting bands are superimposed onto the Ag bulk projected band continuum as shown in Fig. 3(c). The bright yellow bands, with higher intensities, are the original Ag_2Ge bands and the dark-blue bands, with lower intensities, are the unfolded bands. The SBZs and symmetry points of the Ag_2Ge layer (blue) and the $\text{Ag}(111)$ surface (red) are indicated in Fig. 3(b). The calculated, including the original (solid curves) and the unfolded (dashed curves), and the measured bands [Fig. 1(b)] are compared in Fig. 3(d); the match is agreeable for either the S'_1 and S'_2 bands centered at $\bar{\Gamma}$ or the splitting S'_3 bands centered at $\bar{M}_{\text{Ag}(111)}$. Note that the unfolded bands from the calculation match well the left branch of the measured splitting bands at $\bar{M}_{\text{Ag}(111)}$ but hardly find counterparts about $\bar{\Gamma}$ in the data. This is likely due to the very low intensity of the umklapp bands around $\bar{\Gamma}$. The occupied bands dispersing upward from ~ -1 eV at $\bar{\Gamma}$ indicated by an arrow in the calculated result of Fig. 3(c) are also missing from the measured ones in Fig. 3(d). The reason will be addressed later. It is worth noting that two sets of hyperbolic constant-energy contours, which correspond to the splitting bands at $\bar{M}_{\text{Ag}(111)}$, are observed in the bottom panel of Fig. 5(b) of Ref. [22] and Fig. S5 of the Supplemental Material [31]. This indicates that all the bands in the directions parallel to $\bar{\Gamma}\bar{A}_{\text{Ag}_2\text{Ge}} - \bar{K}_{\text{Ag}_2\text{Ge}} - \bar{M}_{\text{Ag}_2\text{Ge}}$ undergo umklapp-scattering effects with $\bar{G}_{\text{Ag}(111)} = 2\bar{\Gamma}_{\text{Ag}(111)}\bar{M}_{\text{Ag}(111)}$.

An intriguing question arises, “How can the Ag_2Ge surface alloy stabilize in spite of a 5% lattice mismatch with the

underlying $\text{Ag}(111)$ surface?” Figure 4(a) shows the measured energy band dispersions of the Pb(111) dense phase in two symmetry directions, $\bar{\Gamma}\bar{M}$ and $\bar{\Gamma}\bar{K}$, after depositing extra Pb atoms onto the Ag_2Pb surface alloy. Note that green (red) symbols indicate the symmetry points of Pb(111) [$\text{Ag}(111)$], as shown from Fig. 4(c) that depict both SBZs. As was reported [34], the Ag_2Pb surface alloy undergoes a dealloying process at a coverage above $1/3$ ML to form the $\text{Pb}(111)\text{-}1 \times 1$ dense phase. In our experimental approach, we found that such a dealloying process can occur at RT without annealing. This implies the metastability of the Ag_2Pb surface alloy since the Pb atoms are only partially immersed in the alloy. Figure 4(d) shows the DFT calculation results on a one-layer freestanding Pb film in all major symmetry directions. The red curves superimposed onto the measured bands in Figs. 4(a) and 4(b) are those from Fig. 4(d) with a 0.6-eV offset. As seen, except for a Λ -shaped Ag bulk projected band edge centered at $\text{Ag}(111)$ SZB, the bands with the orbital characters of p_x and p_y match the measured ones well but the bands of p_z type do not have the counterparts in the measured spectra. The absence of p_z bands in the measured spectra has occurred in several monatomic layers [3,6,35] and it was mainly ascribed to the interaction with the substrate due to the fact that their wave functions are out of the monolayer plane (See Supplemental Material Figs. S3(a) and S3(c) [31]). The same reason explains why the upward band centered at $\bar{\Gamma}$ for Ag_2Ge on $\text{Ag}(111)$ revealed in the calculation, Fig. 3(c), is not observed in the measurement, Fig. 3(d), which is also a p_z type (See Supplemental Material Fig. S4 [31] and Refs. [21,22]). The calculated band structures in Fig. 4(d) show that the p_z bands interact with the $p_x p_y s$ bands to cause a band gap merely above the Fermi level midway between $\bar{\Gamma}$ and the SZBs, but Figs. 4(a) and 4(b) indicate the absence of such

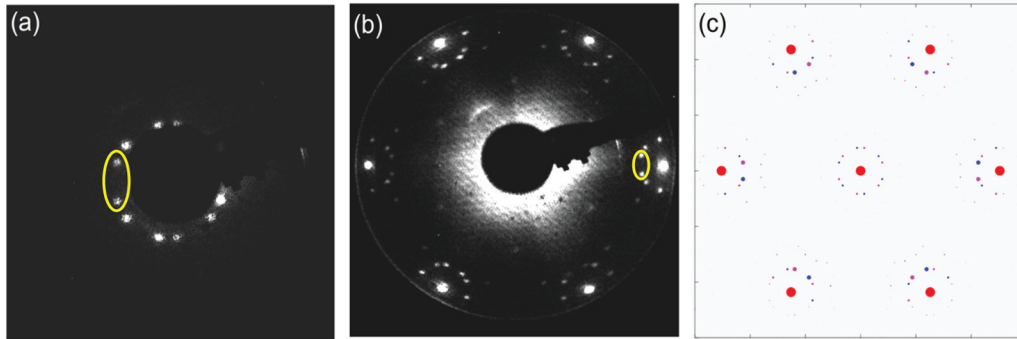


FIG. 5. LEED patterns of a 1-ML Pb(111) dense phase on an Ag(111) surface. (a), (b) Measured LEED patterns of 1-ML Pb(111) dense phase on Ag(111) at electron energy 20 and 45 eV. (c) Simulated LEED patterns of 1-ML Pb(111) layer on Ag(111).

band gaps because p_z bands are pushed out of this energy range [9]. Upon a further close examination, one can also see from Fig. 4(a) a band split at $\vec{M}_{\text{Ag}(111)}$, which looks like a similar type (See Supplemental Material Fig. S2 [31]) to that of Ag_2Ge on Ag(111), except that the splitting magnitude is larger and the more intense branch is at the left rather than at the right of $\vec{M}_{\text{Ag}(111)}$. Therefore, the left belongs to the original Pb band and the right originates from the umklapp scattering mediated by Ag(111). The extracted splitting value, 0.214 \AA^{-1} , between $\vec{M}_{\text{Pb}(111)}$ and $\vec{M}_{\text{Ag}(111)}$ corresponds to a lattice mismatch of 20.6%, close to the value of 20.5% derived from the bulk lattice constants of Pb and Ag, 4.92 and 4.08 Å. The LEED patterns in Fig. 5(a) exhibit 12 Moiré satellite spots around (00). It is actually made of 6 doublets. Each doublet, as enclosed by the yellow oval, spans $\pm 21.5^\circ$ with respect to the (00) point. This is the rotation angle of Moiré symmetry axis with respect to Ag(111). Figure 5(b) shows the same Moiré spots around the (10) points of Ag(111) in addition to the blurred residual spots of the Ag_2Pb layer at $(1/3 \ 1/3)$; however the doublet, as enclosed by the yellow oval, spans $\pm 4^\circ$ with respect to (00). This indicates two domains of 1-ML Pb(111) films rotated $\pm 4^\circ$ with respect to the Ag(111)-1 \times 1 direction. Such a rotating behavior has been found in other film-substrate systems [20,36,37] and is considered as a spontaneous mechanism for reducing large lattice mismatch. Taking in to account the lattice constants of Pb(111) and Ag(111) as well as the $\pm 4^\circ$ splitting of LEED spots, the Moiré spots are reproduced via Eq. (1) as presented in Fig. 5(c). Note that the calculation for energy band dispersions in Fig. 4(d) does not consider the $\pm 4^\circ$ off the symmetry directions. The energy band dispersions close to those directions are shown in Supplemental Material Fig. S3(b) [31], which show no relevant difference from those along symmetry directions.

Both large lattice-mismatched monatomic layers of Ag_2Ge alloy and 1-ML Pb film on Ag(111) show the common feature of the band splits at $\vec{M}_{\text{Ag}(111)}$, generated by umklapp scattering via Ag(111). Such substrate-mediated umklapp electronic states in the context of incommensurate interface were observed as a second kind of quantum-well state (QWS) in Ag films [38,39] or Pb films [20] at a thickness above 1 ML on Ge(111). The discrete momentum perpendicular to the surface, k_\perp , of QWS has to be taken into account for the phase accumulation model although it is the momentum parallel to the surface, k_\parallel , which induces umklapp scattering.

For the case of a monatomic layer, there is no k_\perp of the electronic states so the corresponding energy band structures of the monolayer electrons undergoing the substrate-mediated umklapp effect would be simply offset by the reciprocal vector of the substrate surface, as clearly illustrated in Fig. 2(e). It is worth mentioning that the crossing points of the splitting bands do not reveal relevant band gaps for the Ag_2Ge alloy and 1-ML Pb film on Ag(111) possibly due to a weak superlattice potential [40]. Because the second kind of QWS, as the first kind, partially contribute to the total surface energy of a film, the monolayer-umklapp-electron states likely do so for a monolayer on an incommensurate interface, and are hence related to the monolayer stability. In addition, although an incommensurate interface is not appropriate for the optimal bonding between atoms of films and substrates to substantially reduce energies, partial bonding can still be achieved as evidenced by the absence of the p_z -type band in the measured energy bands of the Ag_2Ge layer and 1-ML Pb on Ag(111).

IV. CONCLUSION

In conclusion, comparing the two systems, Ge and Pb on Ag(111) at the coverage 1/3 ML, a long-time overlooked factor was discovered that the sizes of adsorbate atoms relative to the substrate atoms are relevant to the lattice and electronic structures of the initial alloy layer and likely further affect subsequent overlayers. For Ag_2Pb on Ag(111), the tensile strain induced by the larger Pb-atom size is released by the corrugation to maintain a $\text{Ag}\sqrt{3}\text{-R}30$ commensurate lattice, while for Ag_2Ge on Ag(111), the compressive strain due to the smaller size of the Ge atom leads to $\sim -5\%$ lattice mismatch at the interface where umklapp scattering mediated by Ag(111) causes the observed band split at $\vec{M}_{\text{Ag}(111)}$. This was further confirmed by the similar behavior observed from 1-ML Pb layer on Ag(111). We solve the puzzle of apparent Rashba band splitting at the substrate SZB for the Ag_2Ge surface alloy on Ag(111) in light of the incommensurate interface. The relation among the composite-atom sizes, the strain percentage with respect to Ag(111), and the band-splitting magnitude can be systematically studied by including other Ag_2M families (e.g., $M = \text{Sn}, \text{Bi}, \text{As}$, etc.) for a completely quantitative comparison (See Supplemental Material Table S1 [31]).

ACKNOWLEDGMENTS

We thank Ku-Ding Tsuei for arranging beam time in the National Synchrotron Radiation Research Center (NSRRC). This research was supported by the Ministry of Science & Technology of Taiwan (Grant No. MOST 105-2112-M-007-017-MY3 for S.-J.T, Grant No. MOST 104-2112-M-002-013-MY3 for W.W.P., and Grant No. MOST

103-2112-M-007-018-MY3 for H.-T.J.). H.-T.J. acknowledges NCHC, CINC-NTU and NCTS, Taiwan, for technical support. We also acknowledge support from the Center for Quantum Technology within the framework of the Higher Education Sprout Project by the Ministry of Education (MOE) in Taiwan.

S.C., A.H., and T.-Y.C. contributed equally to this work.

- [1] A. Molle, C. Grazianetti, Li Tao, D. Taneja, Md. Hasibul Alam, and Deji Akinwande, *Chem. Soc. Rev.* **47**, 6370 (2018).
- [2] P. Vogt, P. De Padova, C. Quaresima, J. Avila, E. Frantzeskakis, M. C. Asensio, A. Resta, B. Ealet, and G. L. Lay, *Phys. Rev. Lett.* **108**, 155501 (2012).
- [3] C.-H. Lin, A. Huang, W. W. Pai, W.-C. Chen, T.-Y. Chen, T.-R. Chang, R. Yukawa, C.-M. Cheng, C.-Y. Mou, I. Matsuda, T.-C. Chiang, H.-T. Jeng, and S.-J. Tang, *Phys. Rev. Mater.* **2**, 024003 (2018).
- [4] A. Acun, L. Zhang, P. Bampoulis, M. Farmanbar, A. Van Houselt, A. N. Rudenko, M. Lingenfelder, G. Brocks, B. Poelsema, M. I. Katsnelson, and H. J. W. Zandvliet, *J. Phys. Condens. Matter* **27**, 443002 (2015).
- [5] J. Yuhara, Y. Fujii, K. Nishino, N. Isobe, M. Nakatake, L. Xian, A. Rubio, and G. Le Lay, *2D Mater.* **5**, 025002 (2018).
- [6] F. F. Zhu, W. J. Chen, Y. Xu, C. L. Gao, D. D. Guan, C. H. Liu, D. Qian, S. C. Zhang, and J. F. Jia, *Nat. Mater.* **14**, 1020 (2015).
- [7] Z. Zhang, E. S. Penev, and B. I. Yakobson, *Chem. Soc. Rev.* **46**, 6746 (2017).
- [8] B. Feng, O. Sugino, R.-Y. Liu, J. Zhang, R. Yukawa, M. Kawamura, T. Iimori, H. Kim, Y. Hasegawa, H. Li, L. Chen, K. Wu, H. Kumigashira, F. Komori, T.-C. Chiang, and S. Meng, I. Matsuda, *Phys. Rev. Lett.* **118**, 096401 (2017).
- [9] F. Reis, G. Li, L. Dudy, M. Bauernfeind, S. Glass, W. Hanke, and R. Thomale, *Science* **357**, 287 (2017).
- [10] R. Ganatra and Q. Zhang, *ACS Nano* **8**, 4074 (2014).
- [11] D. Braga, I. G. Lezama, H. Berger, and A. F. Morpurgo, *Nano Lett.* **12**, 5218 (2012).
- [12] N. Alidoust, G. Bian, S. Y. Xu, R. Sankar, M. Neupane, C. Liu, I. Belopolski, D. X. Qu, J. D. Denlinger, F. C. Chou, and M. Z. Hasan, *Nat. Commun.* **5**, 5136 (2014).
- [13] S. Tang, C. Zhang, Di. Wong, Z. Pedramrazi, H. Z. Tsai, C. Jia, B. Moritz, M. Claassen, H. Ryu, S. Kahn, J. Jiang, H. Yan, M. Hashimoto, D. Lu, R. G. Moore, C. C. Hwang, C. Hwang, Z. Hussain, Y. Chen, M. M. Ugeda, Z. Liu, X. Xie, T. P. Devereaux, M. F. Crommie, S. K. Mo, and Z.-X. Shen, *Nat. Phys.* **13**, 683 (2017).
- [14] J. K. Huang, J. Pu, C. L. Hsu, M. H. Chiu, Z. Y. Juang, Y. H. Chang, W. H. Chang, Y. Iwasa, T. Takenobu, and L. J. Li, *ACS Nano* **8**, 923 (2014).
- [15] D. H. Keum, S. Cho, J. H. Kim, D. H. Choe, H. J. Sung, M. Kan, H. Kang, J. Y. Hwang, S. W. Kim, H. Yang, K. J. Chang, and Y. H. Lee, *Nat. Phys.* **11**, 482 (2015).
- [16] A. Molle, J. Goldberger, M. Houssa, Y. Xu, S. C. Zhang, and D. Akinwande, *Nat. Mater.* **16**, 163 (2017).
- [17] C.-L. Lin, R. Arafune, K. Kawahara, M. Kanno, N. Tsukahara, E. Minamitani, Y. Kim, M. Kawai, and N. Takagi, *Phys. Rev. Lett.* **110**, 076801 (2013).
- [18] E. Golias, M. Krivenkov, A. Varykhalov, Jaime Sánchez-Barriga, and O. Rader, *Nano Lett.* **18**, 6672 (2018).
- [19] P. Czoschke, Hawoong Hong, L. Basile, and T.-C. Chiang, *Phys. Rev. B* **72**, 075402 (2005).
- [20] S.-J. Tang, C. Y. Lee, C. C. Huang, T. R. Chang, C. M. Cheng, K. D. Tsuei, H. T. Jeng, V. Yeh, and T.-C. Chiang, *Phys. Rev. Lett.* **107**, 066802 (2011).
- [21] W. Wang, H. M. Sohail, J. R. Osiecki, and R. I. G. Uhrberg, *Phys. Rev. B* **89**, 125410 (2014).
- [22] E. Golias, E. Xenogiannopoulou, D. Tsoutsou, P. Tsipas, S. A. Giamini, and A. Dimoulas, *Phys. Rev. B* **88**, 075403 (2013).
- [23] D. Pacilé, C. R. Ast, M. Papagno, C. Da Silva, L. Moreschini, M. Falub, A. P. Seitsonen, and M. Grioni, *Phys. Rev. B* **73**, 245429 (2006).
- [24] G. Kresse and J. Hafner, *Phys. Rev. B* **48**, 13115 (1993).
- [25] G. Kresse and J. Furthmüller, *Phys. Rev. B* **54**, 11169 (1996).
- [26] G. Kresse and J. Furthmüller, *Comput. Mater. Sci.* **6**, 15 (1996).
- [27] J. P. Perdew, K. Burke, and M. Ernzerhof, *Phys. Rev. Lett.* **77**, 3865 (1996).
- [28] G. Kresse and D. Joubert, *Phys. Rev. B* **59**, 1758 (1999).
- [29] P. E. Blöchl, *Phys. Rev. B* **50**, 17953 (1994).
- [30] A. I. Liechtenstein, V. I. Anisimov, and J. Zaanen, *Phys. Rev. B* **52**, R5467(R) (1995).
- [31] See Supplemental Material at <http://link.aps.org/supplemental/10.1103/PhysRevB.99.155408> for additional calculated electronic structures, calculated lattice parameters, and measured 2D constant energy contours.
- [32] J. C. Slater, *J. Chem. Phys.* **41**, 3199 (1964).
- [33] I. M. McLeod, V. R. Dhanak, M. Lahti, A. Matilainen, K. Pussi, and K. H. L. Zhang, *J. Phys.: Condens. Mater.* **23**, 265006 (2011).
- [34] J. Dalmas, H. Oughaddou, G. Le Lay, B. Aufray, G. Tréglia, C. Girardeaux, J. Bernardini, J. Fujii, and G. Panaccione, *Surf. Sci.* **600**, 1227 (2006).
- [35] S. K. Mahatha, P. Moras, V. Bellini, P. M. Sheverdyeva, C. Struzzi, L. Petaccia, and C. Carbone, *Phys. Rev. B* **89**, 201416(R) (2014).
- [36] M. Yakes and M. C. Tringides, *J. Phys. Chem. A* **115**, 7096 (2011).
- [37] H. Li and B. P. Tonner, *Surf. Sci.* **193**, 10 (1988).
- [38] S.-J. Tang, Y. R. Lee, S. L. Chang, T. Miller, and T. C. Chiang, *Phys. Rev. Lett.* **96**, 216803 (2006).
- [39] P. Moras, L. Ferrari, C. Spezzani, S. Gardonio, M. Ležaić, Ph. Mavropoulos, S. Blügel, and C. Carbone, *Phys. Rev. Lett.* **97**, 206802 (2006).
- [40] E. Rotenberg and A. Bostwick, *Synth. Met.* **210**, 85 (2015).